Modeling and Rendering of Weathered Stone

Julie Dorsey   Alan Edelman   Henrik Wann Jensen   Justin Legakis   Hans Køhling Pedersen

Laboratory for Computer Science
Massachusetts Institute of Technology

Abstract

Stone is widespread in its use as a building material and artistic medium. One of its most remarkable qualities is that it changes appearance as it interacts with the environment. These changes are mainly confined to the surface but involve complex volumetric effects such as erosion and mineral dissolution. This paper presents an approach for the modeling and rendering of changes in the shape and appearance of stone.

To represent stone, we introduce a *slab* data structure, which is a surface-aligned volume confined to a narrow region around the boundary of the stone. Our weathering model employs a simulation of the flow of moisture and the transport, dissolution, and recrystallization of minerals within the porous stone volume. In addition, this model governs the erosion of material from the surface. To render the optical effects of translucency and coloration due to the composition of minerals near the surface, we simulate the scattering of light inside the stone using a general subsurface Monte Carlo ray tracer. These techniques can capture many aspects of the time-dependent appearance of stone. We demonstrate the approach with models of granite and marble statues, as well as a sandstone column.

CR Categories: I.3.7 [Computer Graphics]: Three-Dimensional Graphics and Realism; I.6.3 [Simulation and Modeling]: Applications.

Additional Keywords: erosion, material models, natural phenomena, physical simulation, ray tracing, subsurface scattering, texturing, volume modeling, weathering.

1   Introduction

A perennial challenge of computer image generation is the depiction of objects with weathered appearances. Much of the visual richness and ambiance of natural scenes is associated with weathered materials, such as mellowed brickwork, moss-covered masonry, and seasoned timber. Unfortunately, the material models widely used in computer graphics assume that the materials are both pristine and immutable, even though real materials are neither. More sophisticated models would allow materials to change over time as they are exposed to the elements. Such models would then allow for the rendering of convincing images of weathered objects by considering a material's structure, its interaction with light, and the physical processes that affect its appearance.

One of the most important materials for such things as buildings and sculptures is stone, which is ubiquitous across time and place in human history, from the Acropolis to the Washington Monument. As a building material, stone is valuable in part because it is durable, but its durability does not mean that its appearance is static. Each stone has a unique structure and mixture of minerals, and these attributes affect the stone's appearance as it interacts with light. Furthermore, the structure and materials also determine how the stone's appearance and shape will change in the face of the elements.

Figure 2 shows a variety of stones in different stages of decay. Such a range of appearances would be very difficult to model and render with current methods. In this paper, we introduce new techniques for the modeling and rendering of weathered stone.

The complex mechanisms of stone weathering are not fully understood based on first principles; our scientific knowledge is incomplete. But even if we had exact knowledge of those mechanisms, the complicated microscopic and macroscopic heterogeneities of the interior pores in stone would make it impossible to describe in full detail the process of weathering. Techniques of time and space averaging of heterogeneities have allowed scientists to derive equations that model flow and transport in porous and fractured rock. These equations form the basis of our simulation model.

Our approach consists of three major components: a surface-aligned, volumetric data structure that represents a region near the boundary of the surface and serves as the basis for simulations; a simulation to model the flow of water, as well as the transport and dissolution of minerals within the volume and erosion of the surface; and a rendering technique to simulate the subsurface scattering of light. Taken together, these techniques are capable of capturing a wide range of time-dependent appearances.

1.1   Related Work

Previous related work exists in three categories: volume modeling, surface weathering, and subsurface scattering of light.

In volume modeling, an object is represented as a 3D array of voxels [16]. To accelerate volume rendering and the traversal of a volume, octrees [18] and run-length encoding [17] have been used as means of efficiently storing voxel data, while *shells* have been used to encode the location of high-opacity voxels in the vicinity of the boundary [34]. This latter representation is appealing, as it considers only perimeter voxels, while conveying the impression of a full 3D volume. As stone weathers, the majority of the changes occur in a narrow, volumetric band around the surface. In this work, we introduce a *slab* data structure, which is composed of a thin band of volumetric entities aligned with the surface of an object.

Several different approaches to modeling and/or rendering surface weathering effects have been introduced (see [7] and cited references). Of these techniques, the work of Dorsey and Hanrahan is most closely related to our approach, in that they modeled and rendered both surface and subsurface effects using a stack of layers [7]. In other related work, Curtis *et al.* simulated the effects of watercolor painting on paper fibers [6], and Dorsey *et al.* simulated the effects of water flow on surfaces [8]. Both of these approaches demonstrated the ability to affect the appearance of a surface via water flow simulation. However, all of the above techniques are limited to 2D surface effects. The heuristic model for the erosion

of fractal terrains of Musgrave *et al.* [20] also bears relation to the work described here. We move beyond these approaches by simulating changes to both the shape and appearance properties of a material over time.

Methods for modeling the subsurface scattering of light within materials are also relevant [7, 12]. These approaches assume that the surface is composed of a set of homogeneous layers for which one or more simplified transport equations can be solved. As stone is a non-homogeneous mixture of various grains that are not oriented in layers, this assumption is not valid. To render stone we therefore use a general Monte Carlo subsurface ray tracer that treats the stone as a participating medium [26].

1.2 Overview

The next section describes stone and how it weathers, and shows several characteristic effects that inspired our work. Section 3 gives an overview of our system. Section 4 presents a volumetric representation for stone and a simulation system that produces a range of weathering effects. Section 5 describes a method for rendering the subsurface scattering of light in stone. Section 6 demonstrates the approach on several models. Finally, Section 7 discusses some ideas for future work.

2 Background

In this section, we discuss the nature of stone, the weathering process, and some of the most important characteristic weathering effects.

2.1 Rock and Stone

The vast majority of rocks are composed of two or more different minerals joined together in a tight fabric that characterizes the stone and determines in part the physical and chemical properties, color, and durability [36]. "Rock" becomes "stone" when it is shaped by humans. Rocks and stones are classified into three major groups based on their origin and formation:

- *Igneous* rocks crystallize from a silicate melt under intense heat and pressure. As a result, igneous rocks are extremely compact and durable. Granites, which are visibly granular, are the most common of this group.

- *Sedimentary*, or layered rocks, are formed by the accumulation of inorganic or organic debris of variable size and shape, deposited by mechanical means or by chemical precipitation. An important characteristic of sedimentary rocks is their flat, layered structure, known as bedding or stratification. Sandstone and limestone are the most common sedimentary rocks.

- *Metamorphic* rocks are igneous or sedimentary rocks recrystallized by the effects of temperature and pressure. The process is very slow and often associated with intense folding. Limestone and sandstone become marble; clay and shale become slates. Their tightly packed structure makes metamorphic rocks more durable than sedimentary rocks.

2.2 Stone Weathering Processes

We confine our study to what is generally termed *chemical weathering* — the erosion or dissolution of a stone surface by water and pollutants [1, 30]. We do not consider other types of stone weathering, such as mechanical or biological deterioration.

In chemical weathering, rainwater dissolves oxides of carbon, sulfur, and nitrogen, and this solution acts at various rates on the minerals in the stone [11]. The solution is absorbed into the stone, where it then transforms the original minerals, such as calcite and silicate, which are fairly stable, into gypsum and other clay-like substances that are more soluble in water. By recrystallization at the surface and in depth, and by the incorporation of environmental soot, a weak crust is formed on the stone. As parts of the crust break
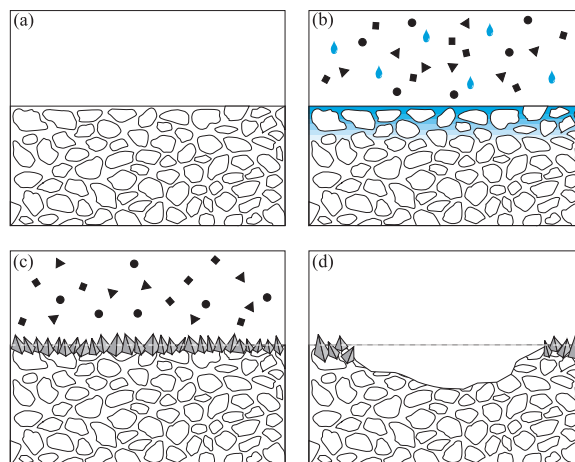

Figure 1 The mechanism of weathering. After a new stone (a) has been exposed to the weather, it comes under attack by oxides that form a solution with rainwater (b). The solution penetrates into the stone and by recrystallization forms a crust (c). If parts of the crust erode (d), new stone is left open to further chemical attack.

off, they carry away with them constituents of the stone, leaving fresh stone open to further chemical attack. Areas that retain water tend to break off first. Thus, horizontal or inclined surfaces erode more rapidly than vertical surfaces [25]. Figure 1 is a schematic diagram of the weathering process.

The net effects of weathering, then, are the formation of dirty crusts, the wearing away of the stone surfaces, and, above all, the loss by the aging stone of its capacity to resist decay. Weathering produces a graded zone in which the properties nearest the surface are altered the most and those farthest from the surface resemble the properties of unweathered stone [1].

The basic processes involved in stone weathering are the travel of moisture, dissolution and recrystallization of minerals, chemical transformation of minerals, and deposition of atmospheric pollutants. These factors are described in more detail below.

- *Travel of moisture*: Among the various elements involved in stone weathering, water is the most critical. As stone is a porous material, water is absorbed into the material by capillary pressure and then evaporated back to the surface. The flow of water over a stone surface also plays a role in the weathering of stone. However, in this work, we focus on modeling the movement of water within the stone itself, which is the principal cause of stone decay [1]. We do, however, model the net effect of the flow of water on the surface using a simple probabilistic approach. Given the time scales in which stone weathering occurs, this gives a reasonable approximation.

- *Dissolution and recrystallization of minerals*: When the minerals and salts that constitute stone come into contact with moisture, they begin to dissolve. The rate of dissolution varies greatly depending on the type of mineral, although it is always very slow by human standards. In general, stones composed of fine grains, such as sandstone, weather more quickly than those with larger grains. As the water evaporates, these dissolved minerals recrystallize.

- *Chemical transformation of minerals*: All minerals occurring in stone undergo a continuous process that transforms them into less durable minerals, and eventually into clay. This process results in changes in the appearance, such as fading, increased roughness, and oxidation of iron traces.
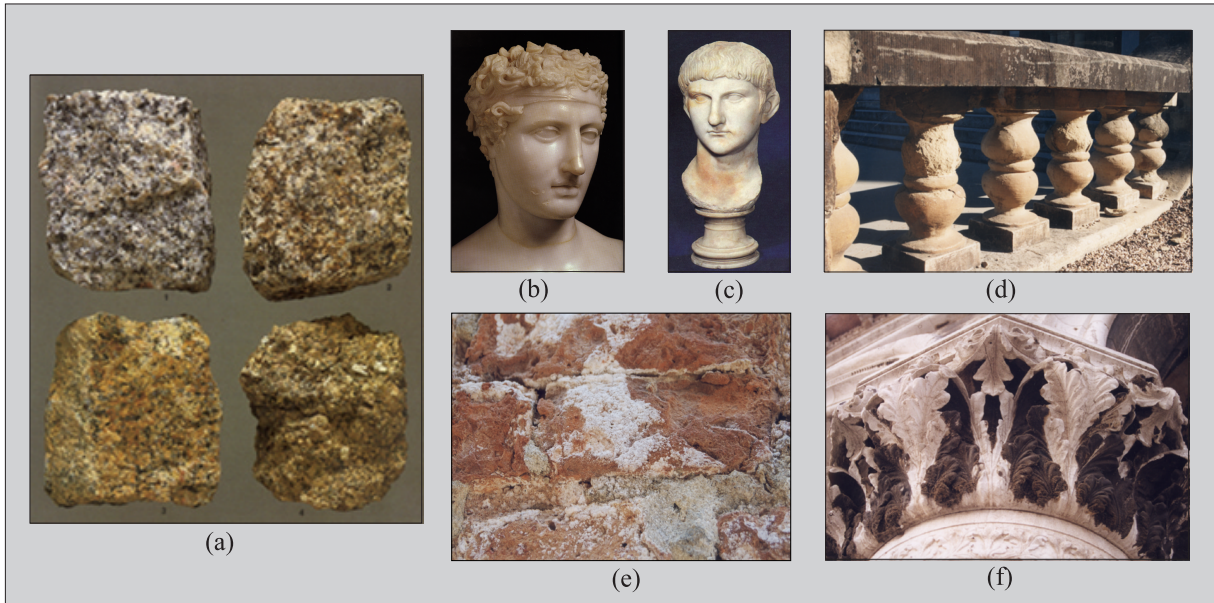
Figure 2 A collection of representative stone weathering effects.

- *Deposition of atmospheric pollution*: The dissolution, re-crystallization, and transformation processes are dramatically accelerated in polluted environments, where atmospheric aerosols, such as sulfur and carbon, act as catalysts. Pollutants can arrive either as airborne deposits or via rain.

2.3 Stone Weathering Effects

The processes described in the previous section come together to produce a variety of characteristic effects. Figure 2 shows a set of photographs that we have collected to document stone weathering.

- *Corestone weathering* (Figure 2a): Compact stones with tightly packed grains tend to weather from their surface inward by transformation of mineral grains into clay. The low porosity makes the material less susceptible to migration of moisture than more porous rocks. The resulting effect is a gradual rounding of sharp corners and loss of high frequency detail [25, 29].

- *Yellowing* (Figure 2a, c, and d): The minerals that constitute stone often contain traces of iron. During the weathering process, the minerals lose iron, which immediately oxidizes. These oxidation products migrate to the surface with the travel of water and are deposited there. This process results in a patchy, yellowish and brownish discoloration [2, 29].

- *Case hardening* (Figure 2d and f): Evaporation moves transformed calcite and other minerals, in the form of clay, toward the surface, leading to case hardening [36], or the build up of a weakened crust on the surface. A variation of this effect, in which the crusts formed on the surface also contain black deposits, is termed *black scabs* [1].

- *Efflorescence* (Figure 2e): Efflorescences are water-soluble salts that crystallize on the surface, forming white or gray deposits. These salts are either present in the material initially or deposited from the atmosphere. They are carried through or onto the surface by moisture [36].

3 System Architecture

Figure 3 presents an overview of our system. The input to our system consists of a polyhedral mesh. We begin by converting the input data into our volumetric slab data structure. From the input mesh, the voxelizer generates a density function for each slab and samples the precomputed dirt and wetness values stored at each mesh vertex. To generate fresh stone, these slabs are passed to the quarry, which samples a 3D stone function for each voxel and scales the result by the density. The simulator operates on the sampled stone data in the slabs to produce weathered stone, affecting both the geometric and chemical makeup of the material.

The volumetric slab data is then used by a subsurface Monte Carlo ray tracer to produce final rendered images. To aid rendering, a polygonal isocontour of the density function is generated to obtain the surface of the weathered stone. In addition, the renderer has direct access to the quarry so that it can sample the various material functions at high resolution.
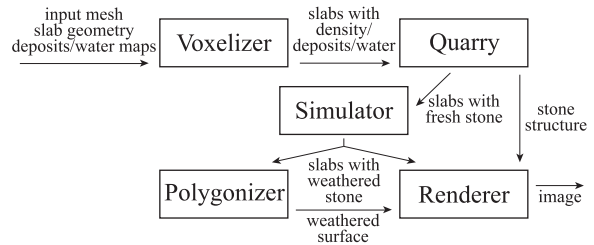

Figure 3 Architecture of the system.

4 Modeling

As we observed in the previous section, the weathering of stone is mainly confined to a thick skin around the surface of an object. In this section, we introduce a volumetric data structure to represent the structure of stone and a simulation model that can be applied to this representation to generate a variety of weathering effects.

4.1 Slabs

We parameterize an object with volumetric entities aligned with the boundary of the model, providing for a thick region encompassing the surface and a domain for the simulations. We call each of these
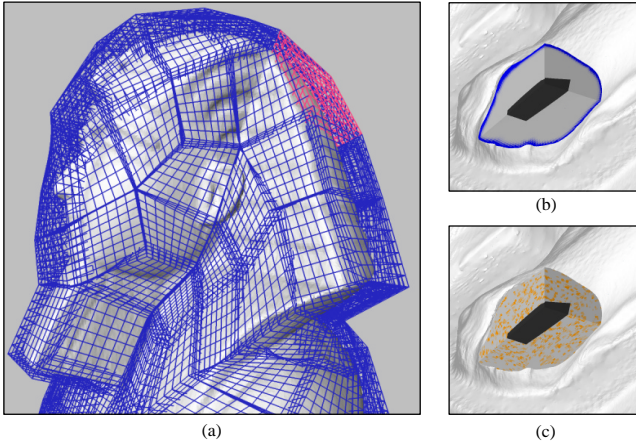
Figure 4 Slab data structure. (a) Slabs on a scanned mesh, (b) Water diffused into the surface, (c) Iron distributed in grains of mica.

entities a *slab*. Slabs combine benefits of surface- and volume-based object representations. In doing so, slabs allow us to constrain our work to the region near the surface of an object, align the coordinate frame with the local orientation of the surface, sample the object beneath the surface, and model geometric changes.

Each slab is a trilinear volume, similar to volumetric textures [15, 21] (see Figure 4). The geometry of each slab is defined by the positions of its eight corners. Inside, these corners define a local (u, v, w) parameter space based on trilinear interpolation between the corner points. Slabs are arranged so that adjacent slabs share four corners, with bilinear patches as their boundaries.

We fit slabs to an object using a set of simple interactive tools. First, we construct a mesh of quadrilateral faces covering a simplified version of the object. This mesh is then extruded, with each face becoming a slab. For smaller slabs, the mesh can be subdivided first. (Catmull-Clark [5] subdivision works well, as it always produces quadrilateral faces.) The four slab edges in the extruded direction are aligned with the average surface normal in the neighborhood of their intersection with the surface. Finally, the slab vertices are edited by hand, to correct any self-intersections or to align individual slabs with specific features of the object.

4.2 Materials

The composition of stone is generated by the *quarry*, in order to provide initial input to the simulations. The input model is first voxelized, creating a sampled density function stored in the slabs. Standard techniques exist for converting meshes into volumetric data sets [28, 35]. As our sampling grid consists of a set of slabs, which are generally distorted and not axis-aligned, this process is slightly more complicated. We sample the density function by computing the signed distance to the input mesh at the corners of each voxel. Voxels completely inside the mesh have density 1, while samples outside the mesh have density 0. Where the surface passes through a voxel, we compute a fractional density value. Given this density function, the quarry generates the remaining parameters to define the fresh, unweathered stone.

To generate the initial stone composition, the quarry uses a combination of standard solid 3D procedural textures [10]. The granular mineral patterns of granite are generated implicitly, similar to Worley's technique for cellular texturing [37]. The veining patterns of marble are created using Perlin's turbulence function [24]. The bedding planes of sandstone are generated using parallel planes distorted by turbulence, to approximate the natural sedimentation processes of layers of different composition building up to form the stone.

4.3 Weathering Simulation

In this section, we describe a simulation model that qualitatively captures many of the effects described in Section 2. This model was constructed by incorporating equations used to model flow and transport in porous media [9, 27], as well as techniques from partial differential equations [32, 33].
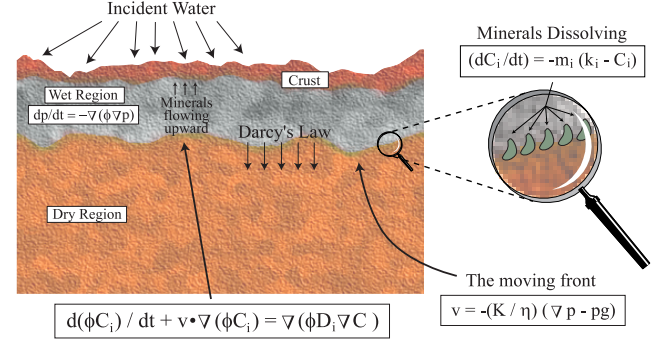

Figure 5 Overview of the simulation model.

4.3.1 Overview

From outside to inside, three locations have special purpose:

- *The stone surface*: This is the two dimensional exterior interface between the stone and the outside environment where 1) water and other external pollutants meet the stone and penetrate the surface and 2) water from the interior of the stone evaporates forming deposits of minerals and salts. This surface suffers erosion with time.

- *The weathered interior*: This is the three dimensional interior volume where water penetrates into the pores and fractures. The water is assumed to hold dissolved minerals and salts. This volume grows during "wet" cycles as more water enters from the surface, and it gets smaller during "dry" cycles as the water evaporates. The volume also is affected by the surface erosion. The longer an element of stone is inside the weathered interior, the more likely it is to weaken and break off.

- *The interior moist/dry front*: This is the boundary of the weathered interior where dry minerals and salts are dissolved by the water.

For easy reference, we provide a list of all the variables and constants indicating precisely how and where they are used in the simulation (see Table 1).

4.3.2 Travel of Moisture

The porous nature of stone allows moisture to be absorbed by capillary pressure during a wet cycle and then evaporated during a dry cycle. These external weathering conditions are modeled by a boundary condition pressure on the stone surface corresponding to the "push" of the water on this surface. In our simulations, we alternate between wet cycles and dry cycles by setting p according to the surface wetness map during the wet cycle and then $p = 0$ during the dry cycle. More generally p on the surface could be a continuous function such as a sine wave. The penetration of water is simulated by a front below the surface. The boundary condition there is always $p = 0$. The further the water penetrates, the more volume that becomes weakened and weathered. The front moves according to Darcy's law

$$v = -\frac{K}{\eta}(\nabla p - \rho g),$$

Symbol	Definition	Loc.*	Comment
C_i	mineral/salt concentration	I	computed by a parabolic operator
d	decay index	V	computed
e	exposure map	S	input and modified
D_i	mineral/salt diffusivity	I	input constant
g	gravity	F	input for Darcy's law
k_i	mineral/salt solubility	I	input constant
m_i	maximum saturation	I	input constant
K	permeability	F	input material constant
p	water pressure	I	computed by evolving parabolic operator
		S	boundary condition derived from exposure map and season
s	stone density	V	input and eroded
v	fluid velocity	I	computed as a pressure gradient
		F	computed by Darcy's law
ϕ	porosity	I	input material constant
ρ	density of water	F	input constant
η	viscosity	F	input constant

*Location key: S=surface, V=volume, F=front, I=interior

Table 1 Parameters for the weathering simulation.

where the velocity v of the front is computed from K, the permeability, η, the viscosity, p, the pressure, ρ, the density, and g, the acceleration due to gravity. Darcy's law roughly states that the velocity of the front is proportional to the negative pressure gradient at the front. Thus, for example, water penetrates further in sandstone than in granite. This is accounted for by the permeability term K.

The location of the water front is computed by evolving the water pressure in time according to the diffusion equation

$$\frac{dp}{dt} = -\nabla \cdot (\phi \nabla p) = -\phi \nabla^2 p - \nabla \phi \cdot \nabla p.$$

The ϕ term is a spatially varying material property indicating the porosity. The wet seasons correspond to turning the pressure p on at the surface; the dry seasons correspond to turning the pressure off. These seasons need not be binary, they can vary continuously. We therefore evolve the moisture through iterations whose inner loop consists of the following two steps:

1. Solve $dp/dt = -\nabla \cdot (\phi \nabla p)$ with pressure p specified as Dirichlet conditions, i.e. the pressure condition is imposed as a boundary condition, on the surface and on the front.

2. Update the front by Darcy's law: $v = -\frac{K}{\eta}(\nabla p - \rho g)$.

4.3.3 Dissolution and Recrystallization of Minerals

The front computed above is the site where minerals and salts first come into contact with water. It is therefore at this front that we calculate the dissolution of any number of minerals and salts. These minerals and salts are assumed transported to the surface by an advection term where they recrystallize forming a crust.

Let C_i denote the concentration in the water of a dissolved mineral or a salt. The dissolution at the front is modeled by the equation

$$\frac{dC_i}{dt} = -k_i(m_i - C_i),$$

where k indicates the solubility of the mineral and m_i is the saturated level, i.e., the maximum solubility. The solubility is a rate constant for the dissolution of the material; the quantity m_i cuts off dissolution upon saturation. We point out that this equation does not have a simple closed form solution because it travels with the front.

Now that the minerals are dissolved, we need to model the movement of minerals to the surface. This is accomplished with the convective-diffusion equation:

$$\frac{\partial}{\partial t}(\phi C_i) + v \cdot \nabla(\phi C_i) = \nabla \cdot (\phi D_i \nabla C_i),$$

where D_i is the diffusivity of the mineral, and v is the velocity as obtained from the pressure gradient.

Finally, minerals and salts form a crust on the surface. The material accumulating on the surface at each time step is ∇C_i. Green's theorem preserves conservation of mass.

4.3.4 Erosion: Transformation to Clay

The presence of stone at a voxel is indicated by a three dimensional stone density function s, whose value is stored in each voxel. The absence of stone is indicated by $s = 0$ at the voxel. The tendency of the stone to transform into clay is indicated by a decay index d that can impact the stone density s in a probabilistic manner.

At every node, a time average of how much water is present is computed. A weighted average of this and various minerals present "weakens" the stone by adding to the decay index d. A large number of erosion events are distributed across the surface with a probability based on the decay index. The density function is reduced within a zone of influence of each event. Once the density hits 0, the stone is no longer present at that site.

4.3.5 Finite Difference Schemes

As the samples inside each slab are arranged in a regular grid, we have chosen a finite difference technique for simplicity. Alternatively, a more complicated finite element method could have been used.

The trapezoidal nature of the lattice of voxels requires special care for the accurate computation of the Laplacian. Carelessly chosen schemes can cause a point source to diffuse into what appears to be more elliptical than an isotropic circle. We have found that a thirteen point scheme is quite adequate.

Our scheme is based on three vectors u, v, and w. The points in the stencil consist of 0, $\pm u$, $\pm v$, $\pm w$ and eight points consisting of sums of any two of $\pm u$, $\pm v$, and $\pm w$.

At the origin, the Laplacian of the functions x^2, y^2, and z^2 is 2, but for other functions such as 1, x, y, z, xy, xz, yz, x^3, $x^2 y$, xy^2, and z^3 the value is 0. If we impose these fourteen conditions on the thirteen points in a least squares manner, we find that this is sufficient to achieve reasonably non-distorted results. Of course more points or smaller mesh sizes could have been incorporated for further accuracy.

The gradient is evaluated as an ordinary finite difference.

5 Rendering

Stone is primarily composed of transparent crystal grains. When light shines upon a crystal it is both reflected and refracted as described by Fresnel's formulae. Light that is refracted into the stone is scattered further due to the large number of grains and the tiny air bubbles and micro-cracks inside and between these grains. The overall result is stones that look opaque but also show a large degree of translucency in thin sections (see Figure 2b). The color of the stone is determined by the type of minerals present [23]. To capture the effect of translucency and the coloration due to minerals, we need to simulate the scattering of light inside the stone. We ignore effects such as diffraction and interference that cannot be handled using geometrical optics. Instead, we treat stone as a participating medium and focus on the simulation of the subsurface scattering of light.

5.1 Subsurface Scattering in Stone

Light transport in a participating medium is described by the following integral-equation [31]:

$$L(x, \vec{\omega}) = \int_{x_e}^{x} \tau(x', x) \, \sigma(x') \int_{\Omega} f(x', \vec{\omega}', \vec{\omega}) \, L(x', \vec{\omega}') \, d\omega' \, dx' + \tau(x_e, x) \, L(x_e, \vec{\omega}) \,, \qquad (1)$$

where $L(x, \vec{\omega})$ is the radiance at x in the direction $\vec{\omega}$, $\sigma(x)$ is the scattering coefficient, $f(x, \vec{\omega}', \vec{\omega})$ is the phase-function describing how light is scattered in different directions, and x_e is the end point of the medium. The transmittance $\tau(x', x)$ from x' to x is given by

$$\tau(x', x) = e^{-\int_{x'}^{x} \kappa(\xi) \, d\xi} \,, \qquad (2)$$

where $\kappa(\xi)$ is the extinction coefficient.

The phase-function f describes how light is scattered within the stone. Since the cracks and air bubbles are larger than the wavelength of light, the type of scattering is described by Mie theory [3]. To simulate the combined effect of back-scattering and forward-scattering, we use the two-lobed Schlick-approximation [4] of the empirical Henyey-Greenstein phase-function [13], which is a good approximation of Mie scattering.

To simulate subsurface scattering in stone, we need to apply a method that can handle the extreme optical thickness of certain stone minerals, such as mica. If we add to this the non-homogeneous media and the non-diffuse phase-function, then it becomes clear that only a method based on Monte Carlo ray tracing will work. We use a variant of the photon map method in which a volume photon map is used to capture the in-scattered light in a participating medium [14].

The volume photon map is generated by emitting photons from the light sources in the scene and storing them as they scatter inside the stone. We only store photons representing the indirect light; the direct light is computed using standard ray tracing techniques.

The rendering method for the stone medium has been integrated in a Monte Carlo based ray tracer. Whenever a ray enters a stone medium it is decided whether the ray interacts with the medium or continues through the medium. The probability of a ray interacting with medium is given by the following cumulative probability density function:

$$P(x_s) = 1 - e^{-\int_{x}^{x_s} \kappa(x') \, dx'} \,. \qquad (3)$$

As stone is non-homogeneous, we use ray marching to compute the value of the integral in this equation. In practice this works by selecting a uniformly distributed random number $0 < \xi < 1$ and computing $\int_{x}^{x_s} \kappa(x') \, dx'$ using ray marching until it equals $-\log \xi$ or until the back of the stone is reached. If the back of the stone is reached it means that no scattering event happened and the ray is traced through the stone. Otherwise a scattering event happened at x_s, and we must compute the radiance L_s scattered in the direction $\vec{\omega}_t$ of the ray at this point. For the extreme optical thickness in stone, this approach is significantly more efficient than the ray marching approach used in [14].

The scattered radiance $L_s(x, \vec{\omega})$ is computed as the sum of out-scattered radiance due to direct illumination L_d and indirect illumination L_i:

$$L_s(x, \vec{\omega}) = L_d(x, \vec{\omega}) + L_i(x, \vec{\omega}) \,. \qquad (4)$$

The out-scattered radiance due to direct illumination is computed by sending a shadow ray to the light source to test for visibility and also to account for extinction (absorption and out-scattering) as the light passes through the stone. The out-scattered radiance due to in-scattered flux is computed using the volume photon map radiance estimate [14]. This is illustrated in Figure 6.
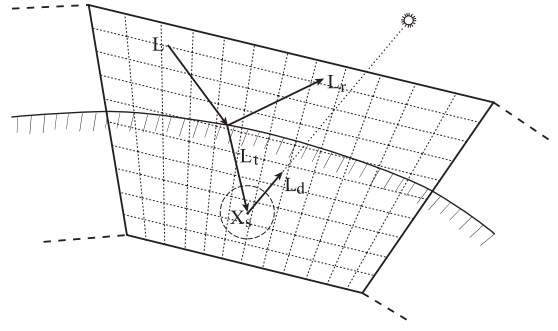

Figure 6 A subsurface scattering event.

The interaction of light with the stone surface is simulated with Fresnel's formulae for unpolarized light entering a dielectric medium. This formula is described in most standard texts on optics e.g. [3]. We compute the amount of reflected light at a surface as $F_r(x, \vec{\omega})^k$, where k serves as a simple approximation of surface roughness. As the surface roughness is increased, the surface will become less reflective, in particular for light entering the surface in a direction close to the surface normal. This has the effect of forcing more light to be scattered below the surface as the roughness is increased. Whenever a ray intersects the stone surface we use this formula to determine the amount of light reflected; the remaining light is transmitted through the surface.

5.2 Integrating the Information in the Slabs

The subsurface rendering method described above does not include the information contained in the slabs. To integrate this information, the ray marcher needs to sample the voxels. The fresh material is still the underlying component since it would be quite costly to make a complete high resolution voxel representation of the stone that is suitable for rendering. Instead, the information in the voxels is used to modify the stone material. This is more efficient since most of the chemical changes within stone are of low frequency.
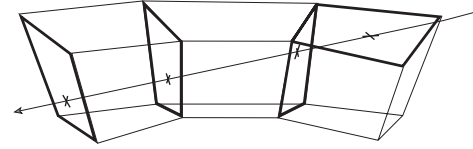

Figure 7 Ray tracing slabs.

To sample the voxels we need to map the points selected by the ray marcher to voxels inside the slabs. To do this, we first build a sorted list of intersected slabs. This list is created by intersecting the ray with the bilinear patch boundaries. The list of boundary intersections is analyzed to match boundaries of the same slab and to generate a list of slab intervals.

The ray marcher uses the sorted list of slabs to keep track of the slab that contains the current sample point (see Figure 7). The data in each slab is sampled based on a linear interpolation between the entry point and the exit point of the ray with the slab. This is similar to the techniques used in [15] and [21]. Here we ignore that a straight line within a slab is a curved line in the real world. Fortunately this distortion is minimal for reasonably shaped slabs.

6 Results

In this section we present results for three models: a granite sphinx, a sandstone column, and a marble statue.

In addition to the models, input to the system consisted of wetness and deposit maps. The deposit maps were computed with accessibility [19] combined with visibility to area deposit sources;

Figure 8 Granite sphinx.

wetness maps were computed with visibility to a directional rain source.

All simulations were run on a quad 250 MHz R10000 SGI machine, and renderings were computed using a dual 400 MHz Pentium II PC running Linux. Images were rendered with global illumination at a resolution of 1024 in the larger dimension, with four samples per pixel.

6.1 Sphinx

Figure 8 shows the weathering of a red granite statue of a sphinx. The model was created from a Cyberware scan and consists of 2.2 million triangles. The model with deposits and wetness maps was then used to initialize 281 slabs, each of which contains 32^3 voxels. The weathering effects in this sequence were created in approximately 24 hours. Figure 4s b and c show representative cross sections of the sphinx with simulations occurring within the interior of the model.

Figure 8a depicts the original statue prior to the weathering simulation. This is a direct rendering of the original mesh using the stone generated by the quarry; rendering time was 31 minutes.

Figure 8b shows the corestone and yellowing effects. Note the loss of high frequency geometric detail and a general roughening of
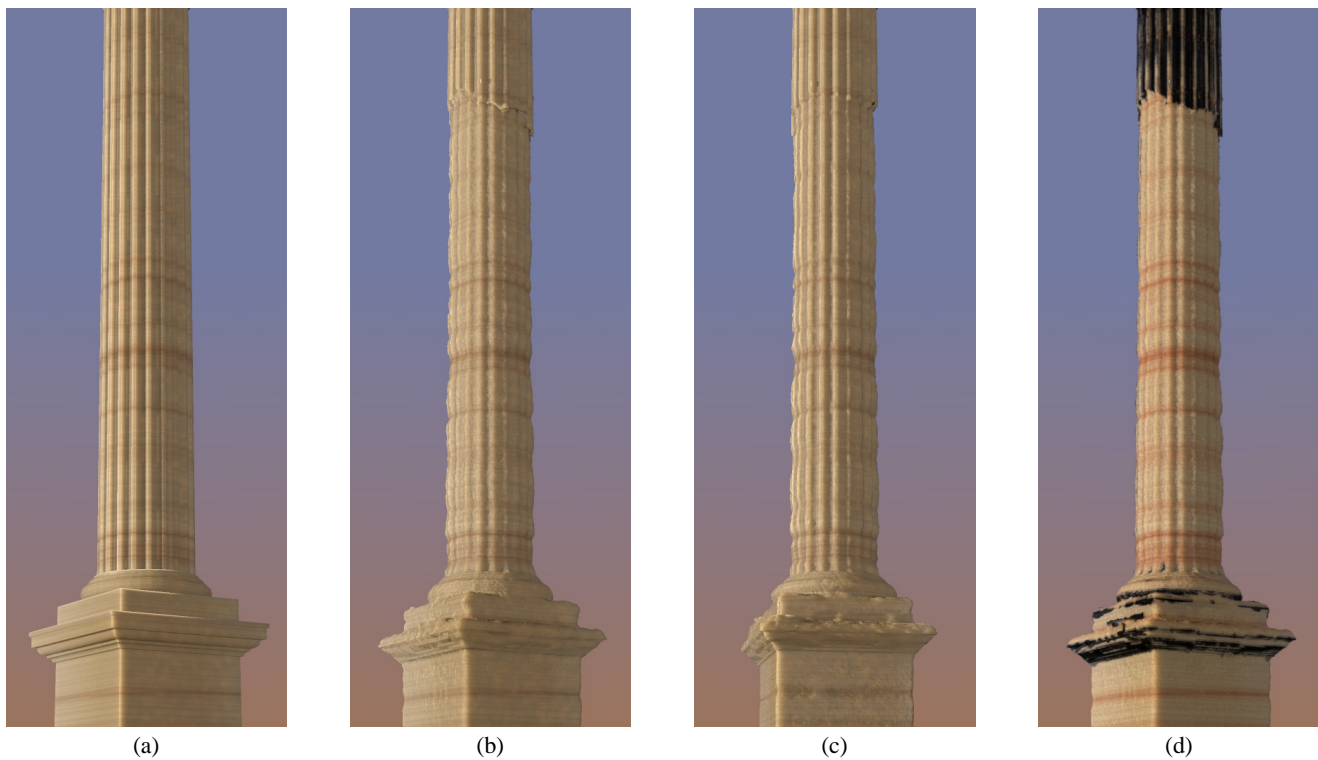
Figure 9 Sandstone column.

the surface. For this simulation, the rain direction was from above, causing the wetness map to be stronger in the horizontal areas. The greater concentration of water and deposits in these areas caused larger amounts of iron deposits to migrate to the surface. Figure 8c shows erosion and efflorescence effects. Salts were applied to the surface with an exposure map during the simulation process. Note the dulling of the surface due to the decay of minerals and recrystallization of salts. 8d shows a more elaborate simulation with both yellowing and efflorescence.

The rendering times for the weathered sphinx were approximately 80 minutes each. This was due mainly to the sampling of the slabs, which we have observed to increase rendering times by a factor of 1 to 10, depending on the complexity of the model. This is mainly due to the conversion from world coordinates to the parameter space of the slab and the intersection of the bilinear patch boundaries of the slabs, which use costly numerical technique.

6.2 Column

Figure 9 shows the weathering of a sandstone column. The column was modeled using AutoCAD and consists of 100,000 triangles. This model consists of 240 slabs, each of which contains 32^3 voxels.

Figure 9a shows the unweathered column. Rendering time was 30 minutes. The dark horizontal bands are bedding planes that were generated by the quarry. These planes consist of weaker, more porous rock with a higher concentration of iron. The simulations in this example were created in approximately four hours.

Figure 9b and 9c show differential erosion of the front and back sides of the column resulting from the weathering simulation. Because the exposure to water and deposits is greater from the front, the erosion is more dramatic on this side. Note that some of the high frequency detail is still present in the vertical flutes on the back side (9c), while the fluting on front side is more eroded.

The bedding planes of varying porosity have a strong impact on the weathering of the sandstone. Note, for example, the strong cor-

relation between the erosion patterns and the layers of the stone. Because the bedding planes have a higher porosity and thus are more permeable than the surrounding stone, the moisture penetrated more deeply and caused the material in these regions to be more susceptible to erosion.

Figure 9d shows both geometric and optical variations. Note the rust-colored regions at the locus of the bedding planes. These were caused by diffusion and recrystallization of dissolved iron. The black regions indicate black scabs that developed on the surface throughout the simulation and slowly moved inward. Note that protected areas retain more carbon than exposed ones. The less eroded region at the top of the column simulates the appearance of the column in a protected region with very little wetness. This effect was achieved by modulating the input wetness map.

6.3 Diana the Huntress

Figure 10 shows simulations on a white marble statue of *Diana the Huntress*, a fourth century B.C. work of art. The model was created from a Cyberware scan and consists of 1.3 million triangles. Figure 11 shows a close-up of the original marble statue prior to the simulations. The light source was placed behind the head to emphasize the simulation of translucency with subsurface scattering. Figure 10a shows the complete model. This image was rendered in 21 minutes. The weathering effects in this example were created in approximately three hours.

Figure 10b shows minor erosion in parts of the statue (concentrated around the right side of the bust, the top of the head, and near the shoulders). Other parts of the sculpture were protected and show less erosion. Note how the yellowing due to dissolved iron is concentrated in the less eroded regions, while whiter, unweathered marble is visible in the more eroded areas. In this example, the case hardening effect is also visible on the surface. Chemical dissolution was the dominant source of erosion in this simulation, although some abrasion also took place in high curvature areas.

(a)   (b)

Figure 10 Marble statue of *Diana the Huntress*.

7   Summary and Discussion

We have described new techniques for the modeling and rendering of weathered stone. We use a surface-aligned, volumetric data structure to represent regions near the boundary of the stone surface. This representation resembles the underlying structure of real stone. We present an approach to simulate the flow of water, the transport and dissolution of minerals within the volume, and the erosion of the surface. We also describe a rendering technique to simulate the subsurface scattering of light. These modeling and rendering techniques are capable of capturing a variety of weathered appearances.

Because the state of our scientific knowledge is incomplete, an exact model for stone weathering is not feasible. Therefore, our model is still a phenomenological one. However, we believe that these techniques have many applications in computer graphics, even if they do not perfectly predict real physical processes. By varying the shape of the objects, the material properties, and the initial conditions of the simulations, we can create strikingly different effects. The metaphor of a volumetric surface — a data structure that combines the benefits of surface- and volume-based representations — is easy to understand and could be used to represent the shape and appearance of many materials.

Our system also suggests several interesting areas for future work. In the examples shown in the paper, we do not exploit fully the potential benefits of the slab data structure. Slabs permit a finer sampling of surface detail compared to axis-aligned voxels; however, the efficiency of the representation would be much more apparent when applied to more complex 3D models, such as a building model, where the use of axis-aligned voxels would be impractical.

The slab data structure could be extended in many ways. For example, we would like to develop a multiresolution version in which we independently vary tangential and perpendicular sampling resolutions, as well as vary the sampling resolution in different parts of the model. We would also like to extend our simulation techniques to include a fracture model [22]. Finally, the basic simulation framework could also be applied to other types of materials that exhibit complex internal structures.

In our current implementation, we generate initial stone samples with standard procedural texturing techniques. An interesting future direction would be to synthesize 3D stone samples directly from real stone. Alternatively, the simulation and rendering of the stone formation process itself would make for a valuable study that could draw on the geology literature.

The material models widely used in computer graphics today are based on the physics of idealized surfaces. However, such idealized materials rarely exist in real life. What is needed are physically-based models of real materials that can sustain a range of appearances over time. Although our simulations show many effects new to computer graphics and demonstrate — to some extent — the potential of combining simulations with better material representations, a comparison between the real and synthetic examples suggests that many challenging problems lie ahead.

Figure 11 Closeup of the unweathered *Diana the Huntress* showing subsurface scattering of light.

References

[1] Giovanni G. Amoroso and Vasco Fassina. *Stone Decay and Conservation*. Elsevier, New York, NY, 1983.

[2] John Ashurst and Francis Dimes, editors. *Conservation of Building and Decorative Stone*. Butterworth-Heinemann, London, 1990.

[3] Michael Bass, editor. *Handbook of Optics*. McGraw-Hill, Inc., New York, NY, 1995.

[4] Philippe Blasi, Bertrand Le Saec, and Christophe Schlick. A rendering algorithm for discrete volume density objects. In R. J. Hubbold and R. Juan, editors, *Eurographics '93*, pages 201–210, Oxford, UK, 1993. Eurographics, Blackwell Publishers.

[5] E. Catmull and J. Clark. Recursively generated B-spline surfaces on arbitrary topological meshes. *Computer-Aided Design*, 10:350–355, September 1978.

[6] Cassidy J. Curtis, Sean E. Anderson, Joshua E. Seims, Kurt W. Fleischer, and David H. Salesin. Computer-generated watercolor. In *Computer Graphics Proceedings*, Annual Conference Series, pages 421–430. ACM SIGGRAPH, August 1997.

[7] Julie Dorsey and Pat Hanrahan. Modeling and rendering of metallic patinas. In *Computer Graphics Proceedings*, Annual Conference Series, pages 387–396. ACM SIGGRAPH, August 1996.

[8] Julie Dorsey, Hans Køhling Pedersen, and Pat Hanrahan. Flow and changes in appearance. In *Computer Graphics Proceedings*, Annual Conference Series, pages 411–420. ACM SIGGRAPH, August 1996.

[9] F. A. L. Dullien. *Porous Media: Fluid Transport and Pore Structure*. Academic Press, New York, NY, second edition, 1992.

[10] David S. Ebert, editor. *Texturing and Modeling*. Academic Press, New York, 1994.

[11] K. Lal Gauri. The preservation of stone. *Scientific American*, 238(6):126–136, June 1978.

[12] Pat Hanrahan and Wolfgang Krueger. Reflection from layered surfaces due to subsurface scattering. In *Computer Graphics Proceedings*, Annual Conference Series, pages 165–174. ACM SIGGRAPH, August 1993.

[13] L. G. Henyey and J. L. Greenstein. Diffuse radiation in the galaxy. *Astrophysics Journal*, 93:70–83, 1941.

[14] Henrik Wann Jensen and Per H. Christensen. Efficient simulation of light transport in scenes with participating media using photon maps. In *Computer Graphics Proceedings*, pages 311–320. ACM SIGGRAPH, August 1998.

[15] James T. Kajiya and Timothy L. Kay. Rendering fur with three dimensional textures. In *Computer Graphics (SIGGRAPH '89 Proceedings)*, volume 23, pages 271–280, July 1989.

[16] Arie Kaufman, Daniel Cohen, and Roni Yagel. Volume graphics. *IEEE Computer*, 26(7):51–64, July 1993.

[17] Philippe Lacroute and Marc Levoy. Fast volume rendering using a shear–warp factorization of the viewing transformation. In *Computer Graphics Proceedings*, Annual Conference Series, pages 451–458. ACM SIGGRAPH, July 1994.

[18] Marc Levoy. Efficient ray tracing of volume data. *ACM Transactions on Graphics*, 9(3):245–261, July 1990.

[19] Gavin Miller. Efficient algorithms for local and global accessibility shading. In *Proceedings of SIGGRAPH '94*, Annual Conference Series, pages 319–326, July 1994.

[20] F. Kenton Musgrave, Craig E. Kolb, and Robert S. Mace. The synthesis and rendering of eroded fractal terrains. *Computer Graphics*, 23(3):41–50, July 1989.

[21] Fabrice Neyret. Modeling, animating, and rendering complex scenes using volumetric textures. *IEEE Transactions on Visualization and Computer Graphics*, 4(1), January – March 1998.

[22] James F. O'Brien and Jessica K. Hodgins. Graphical modeling and animation of brittle fracture. In *Computer Graphics Proceedings*. ACM SIGGRAPH, August 1999.

[23] Andrew Peckett. *The Colours of Opaque Minerals*. John Wiley and Sons Ltd, Chichester, England, 1992.

[24] Ken Perlin. An image synthesizer. In B. A. Barsky, editor, *Computer Graphics (SIGGRAPH '85 Proceedings)*, volume 19, pages 287–296, July 1985.

[25] D. G. Price. Weathering and weathering processes. *Quarterly Journal of Engineering Geology*, 16(28):243–252, June 1995.

[26] Holly E. Rushmeier. *Realistic Image Synthesis for Scenes with Radiatively Participating Media*. Phd thesis, Cornell University, 1988.

[27] Muhammad Sahimi. *Flow and Transport in Porous Media and Fractured Rock*. VCH, New York, NY, 1995.

[28] William J. Schroeder and William E. Lorensen. Implicit modeling of swept surfaces and volumes. In *Visualization '94*, pages 40–45. IEEE, IEEE Computer Society Press, October 1994.

[29] Walter Schumann. *Handbook of Rocks, Minerals, and Gemstones*. HarperCollins Publishers and Houghton Mifflin Company, New York, NY, 1993.

[30] M. J. Selby. *Hillslope Materials and Processes*. Oxford University Press, Oxford, England, 1993.

[31] Robert Siegel and John R. Howell. *Thermal Radiation Heat Transfer*. Hemisphere Publishing Corporation, Washington, D.C., 3rd edition, 1992.

[32] Gilbert Strang. *Introduction to Applied Mathematics*. Wellesley-Cambridge Press, Wellesley, MA, 1986.

[33] John C. Strikwerda. *Finite Difference Schemes and Partial Differential Equations*. Wadsworth and Brooks, Pacific Grove, CA, 1989.

[34] Jayaram K. Udupa and Dewey Odhner. Shell rendering. *IEEE Computer Graphics and Applications*, 13(6):58–67, November 1993.

[35] Sidney W. Wang and Arie E. Kaufman. Volume-sampled 3d modeling. *IEEE Computer Graphics and Applications*, 14:26–32, September 1994.

[36] Erhard M. Winkler. *Stone in Architecture: Properties, Durablity*. Springer-Verlag, New York, NY, 1997.

[37] Steven P. Worley. A cellular texture basis function. In *SIGGRAPH 96 Conference Proceedings*, Annual Conference Series, pages 291–294. ACM SIGGRAPH, August 1996.